

Valley polarization in 2D tetragonal altermagnetism

San-Dong Guo^{1,*}, Xiao-Shu Guo¹, and Guangzhao Wang²

¹*School of Electronic Engineering, Xi'an University of Posts and Telecommunications, Xi'an 710121, China and*

²*Key Laboratory of Extraordinary Bond Engineering and Advanced Materials Technology of Chongqing, School of Electronic Information Engineering, Yangtze Normal University, Chongqing 408100, China*

The altermagnetism caused by alternating crystal environment provides a unique opportunity for designing new type of valley polarization. Here, we propose a way to realize valley polarization in two-dimensional (2D) tetragonal altermagnetism by regulating the direction of magnetization. The valley polarization along with spin polarization will arise when the orientation of magnetization breaks the C_{4z} lattice rotational symmetry, particularly in the conventional in-plane x or y directions. When the direction of magnetization switches between the x and y direction, the valley and spin polarizations will be reversed. This is different from the widely studied valley polarization, which occurs in out-of-plane hexagonal magnetic materials with valley physics at $-K/K$ point. Followed by first-principles calculations, our proposal is demonstrated in a 2D Janus tetragonal altermagnetic $\text{Fe}_2\text{MoS}_2\text{Se}_2$ monolayer with good stability but very small valley splitting of 1.6 meV. To clearly see the feasibility of our proposal, an unrealistic material $\text{Ru}_2\text{MoS}_2\text{Se}_2$ is used to show large valley splitting of 90 meV. In fact, our proposal can be readily extended to 2D tetragonal ferromagnetic (FM) materials, for example FM Fe_2I_2 monolayer. Our findings can enrich the valley physics, and provide new type of valley materials.

INTRODUCTION

Valley, characterizing the energy extrema of band, provides a new degree of freedom to process information and perform logic operations with low power consumption and high speed, and this entity is referred to as valleytronics[1–4]. To make use of valley degree, the crucial step is to break the balance of the number of carriers between the valleys, known as valley polarization[5–9]. Two-dimensional (2D) magnetic materials provide the new opportunity for the long-sought spontaneous valley polarization[10]. In previous most works, spontaneous valley polarization is generally considered to occur in 2D hexagonal ferromagnetic (FM) materials with out-of-plane magnetization[11–20], and the valley physics is concentrated at $-K/K$ point in the Brillouin zone (BZ). Compared with ferromagnetism, antiferromagnetic (AFM) materials possess zero magnetic moment, which are inherently robust to external magnetic perturbation, and possess ultrafast dynamics[21, 22], thus providing enormous potential for device applications. In fact, the spontaneous valley polarization can also occur in hexagonal AFM monolayers[23, 24], but missing spin splitting in the band structures prevents some interesting physical phenomena.

Altermagnetism is a recently discovered third class of collinear magnetism, which shares some properties with AFM ordering (zero magnetic moment) and even more with FM ordering (spin splitting)[25, 26]. The zero-magnetization magnetic structures of altermagnetism is special-symmetry-driven, for example rotational and mirror symmetries rather than translational and inversion symmetries. The altermagnetic spin splitting arises in the zero spin-orbital coupling (SOC) limit. Achieving valley polarization in altermagnetism may be significant

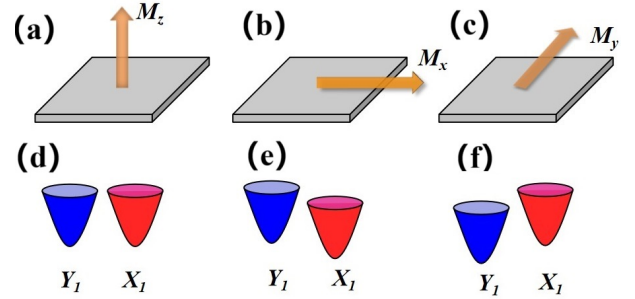


FIG. 1. (Color online) (a): 2D tetragonal out-of-plane altermagnetism possesses equivalent valleys Y_1 and X_1 (d) with opposite spin character along Γ -Y and Γ -X lines in the BZ; (b): When the direction of magnetization is in-plane along the x direction, the Y_1 and X_1 valleys become unequal (e), giving rise to valley polarization along with spin polarization; (c): When rotating the magnetization direction from x to y , the transformation of valley and spin polarizations can be achieved (f). In (d,e,f), the spin-up and spin-down channels are depicted in blue and red.

and interesting for constructing new type of valleytronic device. The valley can be polarized by simply breaking the corresponding crystal symmetry with uniaxial strain in tetragonal lattice[27–31]. Recently, twisted altermagnetism has been proposed by introducing a key in-plane 2-fold rotational operation, and the symmetry of spin splitting, i.e., d -wave, g -wave or i -wave, can be realized by choosing out-of-plane rotational symmetry[32]. The twisted altermagnetism can possess valley-layer coupling, and an out-of-plane external electric field can be used to induce valley polarization[33, 34].

In this work, we propose the realizability of valley polarization in 2D tetragonal altermagnetism. The physics of the proposed way is rooted in the combination of SOC

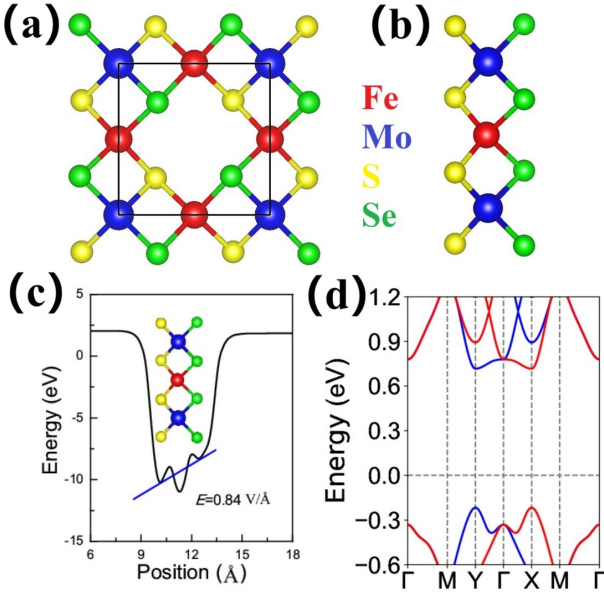


FIG. 2. (Color online) For $\text{Fe}_2\text{MoS}_2\text{Se}_2$, (a) and (b): top and side views of the crystal structures; (c): planar averaged electrostatic potential energy variation along z direction. E stands for the intrinsic polar field; (d): the energy band structures without SOC. The spin-up and spin-down channels are depicted in blue and red.

and in-plane magnetization. By rotating in-plane magnetization, the valley polarization can be reversed at intervals of 90° . Based on first-principles calculations, this way is validated in a 2D Janus tetragonal altermagnetic $\text{Fe}_2\text{MoS}_2\text{Se}_2$ with good stability and an unrealistic material $\text{Ru}_2\text{MoS}_2\text{Se}_2$. Therefore, the valley design by tuning magnetization in altermagnets would bring rich designability to valleytronics.

APPROACH AND MATERIAL REALIZATION

The spontaneous valley polarization is generally considered to occur in 2D hexagonal magnetic lattice (both FM and AFM systems) with valley physics at $-K/K$ point [10–20, 23, 24], and the SOC and d orbital characteristics play dominated role for generating the valley polarization. For $d_{x^2-y^2}/d_{xy}$ -dominated $-K/K$ valley, in the general magnetization direction $M(\theta, \phi)$ [Polar angles θ and ϕ define the magnetization orientation], the valley splitting $\Delta E_{VS} = 4\alpha \cos\theta$ [20], where the α is SOC-related constant, and the $\theta=0/90^\circ$ means out-of-plane/in-plane magnetization direction. The in-plane magnetization with collinear magnetic ordering forbids the existence of valley polarization [20]. For out-of-plane case, only $d_{x^2-y^2}/d_{xy}$ -orbital-dominated $-K$ and K valleys show obvious valley splitting.

Here, we assume that a 2D tetragonal altermagnetism possesses two valleys Y_1 and X_1 along Γ -Y and Γ -X lines

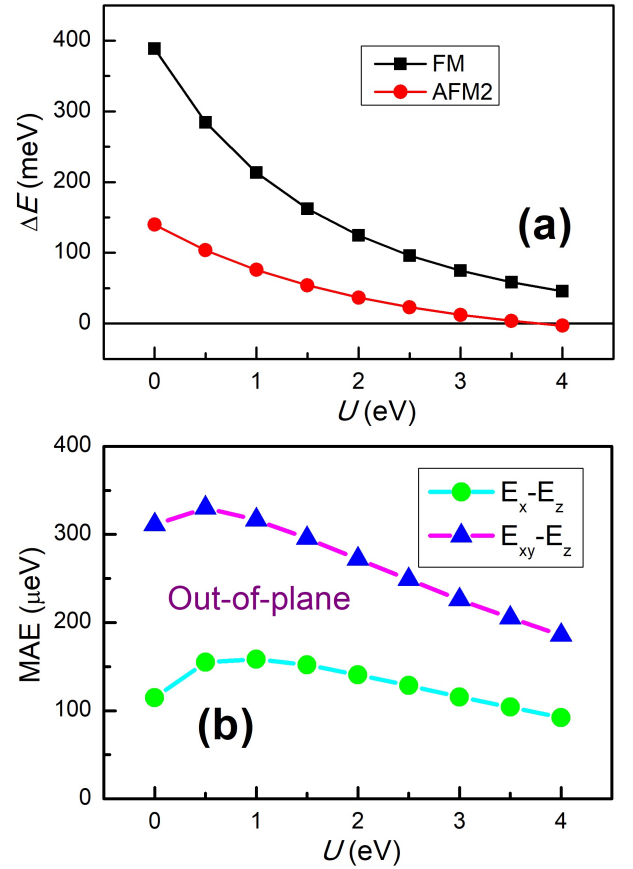


FIG. 3. (Color online) For $\text{Fe}_2\text{MoS}_2\text{Se}_2$, the energy differences per unit cell between FM/AFM2 and AFM1 (a) and MAE (b) as a function of U .

in BZ, which have opposite spin character. The two valleys have no valley polarization due to C_{4z} lattice symmetry in absence of SOC. While the spin splitting is present, there is an absence of spin polarization due to spin-valley locking. With SOC, the magnetization direction has important effects on electronic structures of tetragonal altermagnetism by changing magnetic group symmetry (the lattice symmetry combined with time reversal symmetry T). When the system has an out-of-plane magnetization, the magnetic point group symmetry $C_{4z}T$ forbids the existence of valley polarization (Figure 1 (a) and (d)). In other words, the x and y axes (Γ -Y and Γ -X directions in BZ) are equivalent. With in-plane magnetization along x direction, the $C_{4z}T$ symmetry will be broken, producing valley and spin polarizations (Figure 1 (b) and (e)). When in-plane magnetization direction changes from x to y , the valley and spin polarizations will be reversed (Figure 1 (c) and (f)).

If the magnetization is in the general direction $M(\theta, \phi)$, no valley polarization is produced, provided that the projections $M_x(90^\circ, 0^\circ)$ and $M_y(90^\circ, 90^\circ)$ are equivalent. So, when $\theta=0^\circ, 180^\circ$ or $\phi=45^\circ, 135^\circ, 225^\circ, 315^\circ$, the valley polarization will disappear. The valley splitting can be

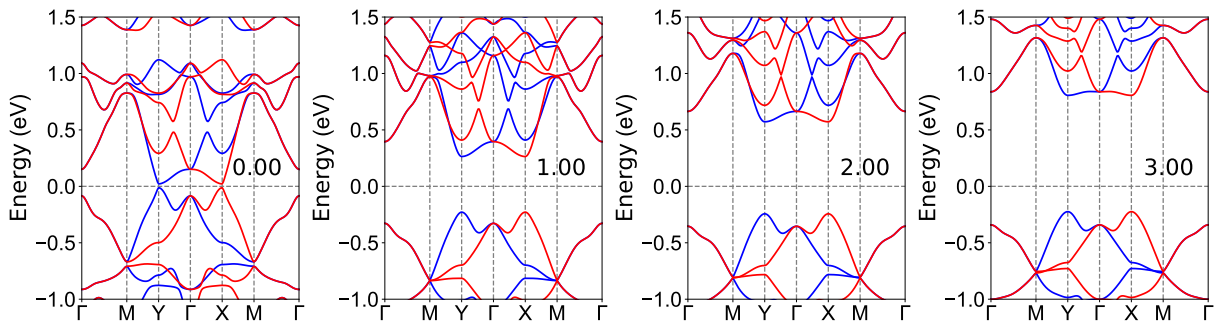


FIG. 4. (Color online) For $\text{Fe}_2\text{MoS}_2\text{Se}_2$, the energy band structure without SOC at representative U values ($U=0, 1, 2, 3$ eV).

defined as $\Delta E_{VS} = E_{Y_1} - E_{X_1}$, which oscillates between positive and negative values at intervals of 90° for ϕ (see FIG.S1 of electronic supplementary information (ESI)).

Monolayer Cr_2O_2 , Cr_2SO , $\text{V}_2\text{Se}_2\text{O}$, V_2SeTeO and $\text{Fe}_2\text{Se}_2\text{O}$ [27–31] can be used to prove our proposal. These monolayers are tetragonal altermagnetism with equivalent valleys along Γ -X and Γ -Y lines in the BZ without SOC. Instead of available tetragonal altermagnets, we predict a new Janus tetragonal altermagnet $\text{Fe}_2\text{MoS}_2\text{Se}_2$ with good stability. We will use $\text{Fe}_2\text{MoS}_2\text{Se}_2$ as a prototype system to illustrate the proposal of in-plane magnetization induced valley polarization in 2D tetragonal altermagnetism. The first-principles calculation method is used to prove our proposal.

COMPUTATIONAL DETAIL

Within density functional theory (DFT)[35], the spin-polarized first-principles calculations are carried out within Vienna ab initio Simulation Package (VASP)[36–38] by using the projector augmented-wave (PAW) method. The exchange-correlation potential is adopted by generalized gradient approximation of Perdew-Burke-Ernzerhof (PBE-GGA)[39]. A kinetic energy cutoff of 500 eV, total energy convergence criterion of 10^{-8} eV, and force convergence criterion of $0.0001 \text{ eV} \cdot \text{\AA}^{-1}$ are set to obtain reliable results. To account for electron correlation of Fe-3d orbitals, a Hubbard correction is employed within the rotationally invariant approach proposed by Dudarev et al. The vacuum slab of more than 16 \AA is applied to avoid the physical interactions of periodic cells. A $12 \times 12 \times 1$ Monkhorst-Pack k-point meshes is used to sample the BZ for calculating electronic structures. The phonon dispersion spectrum is obtained by the Phonopy code[40] within finite displacement method by using $4 \times 4 \times 1$ supercell. The ab-initio molecular dynamics (AIMD) simulations using NVT ensemble are performed for more than 8000 fs with a time step of 1 fs by using a $3 \times 3 \times 1$ supercell. The elastic stiffness tensor C_{ij} are calculated by using strain-stress relationship, which have been renormalized by $C_{ij}^{2D} = L_z C_{ij}^{3D}$, where the L_z

is the length of unit cell along z direction.

CRYSTAL STRUCTURE AND STABILITY

Monolayer $\text{Fe}_2\text{MoS}_2\text{Se}_2$ has a square lattice structure with the space group $Cmm2$ (No.35). As shown in Figure 2 (a) and (b), $\text{Fe}_2\text{MoS}_2\text{Se}_2$ contains three atomic sublayers with one Mo and two Fe atoms as middle layer and S/Se atoms as upper and lower layers, which can be constructed by replacing one of two Se layers with S atoms in monolayer Fe_2MoSe_4 [41]. To determine the magnetic ground states, the FM and two AFM configurations (AFM1 and AFM2) are constructed from a $\sqrt{2} \times \sqrt{2} \times 1$ supercell, as shown in FIG.S2 of ESI. The AFM1 configuration can show altermagnetism, which can be reduced into crystal primitive cell, including two Fe atoms with opposite spin. The GGA+ U (The $U=2.5$ eV is adopted[42].) results show that the AFM1 ordering is magnetic ground state, and its energy is 96/23 meV lower than that of FM/AFM2 case. The optimized lattice constants are $a=b=5.576 \text{ \AA}$ by GGA+ U for AFM1 case. The magnetic easy-axis can be determined by magnetic anisotropy energy (MAE), which can be obtained by calculating the energy difference of the magnetization orientation along the (100)/(110) and (001) cases. Calculated results show that the MAE is 129/249 $\mu\text{eV}/\text{Fe}$, indicating that the easy-axis of $\text{Fe}_2\text{MoS}_2\text{Se}_2$ is out-of-plane.

To explore the stability of $\text{Fe}_2\text{MoS}_2\text{Se}_2$, the phonon dispersion, AIMD and elastic constants are performed by using GGA+ U for AFM1 case. According to FIG.S3 of ESI, the phonon dispersions show no obvious imaginary frequencies, indicating the dynamic stability of $\text{Fe}_2\text{MoS}_2\text{Se}_2$. To corroborate the thermal stability, the total energy as a function of simulation time is shown in FIG.S4 of ESI using AIMD at 300 K. It is suggested that the thermal-induced energy fluctuations and changes in geometry are small, indicating that the $\text{Fe}_2\text{MoS}_2\text{Se}_2$ has good thermal stability at room temperature. For $\text{Fe}_2\text{MoS}_2\text{Se}_2$, the independent elastic constants are $C_{11}=48.67 \text{ Nm}^{-1}$, $C_{12}=3.88 \text{ Nm}^{-1}$ and $C_{66}=6.35$

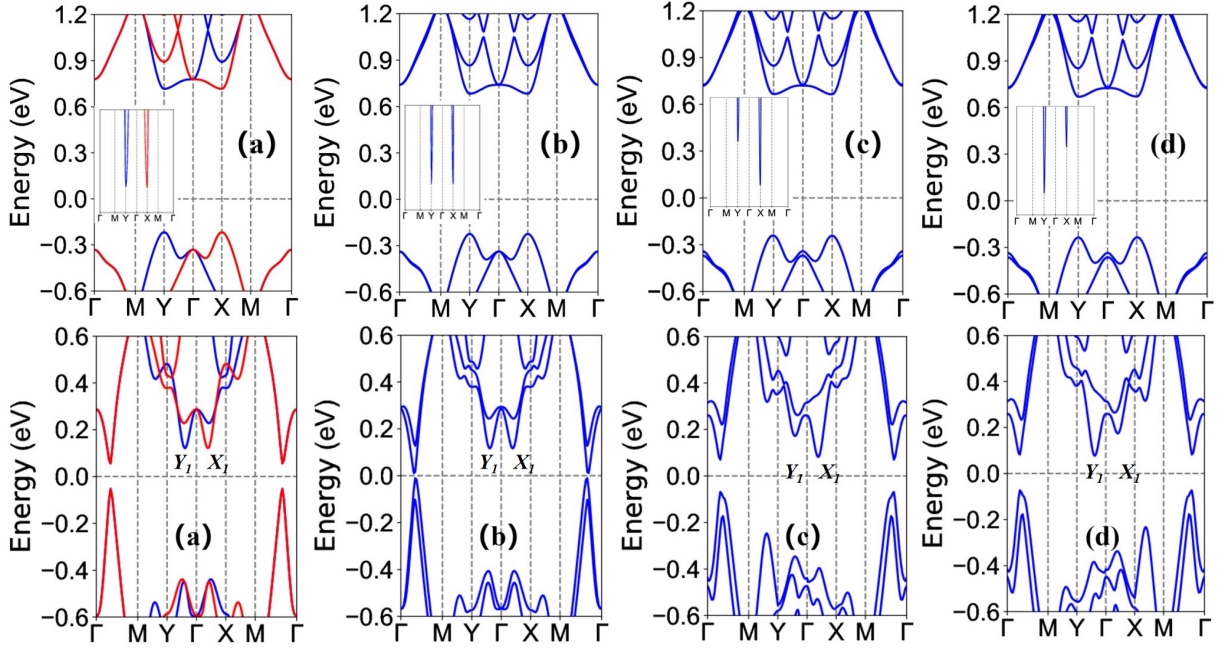


FIG. 5. (Color online) For $\text{Fe}_2\text{MoS}_2\text{Se}_2$ (top) and $\text{Ru}_2\text{MoS}_2\text{Se}_2$ (bottom), the energy band structures without SOC (a), and with SOC (b, c, d) for magnetization direction along the positive z , positive x , and positive y direction, respectively. In (a), the blue (red) lines represent the band structure in the spin-up (spin-down) direction. For top plane, the insets show the enlarged portion of conduction bands near the Fermi energy level.

Nm^{-1} , which satisfy the Born criteria of mechanical stability: $C_{11} > 0$, $C_{66} > 0$, $C_{11} - C_{12} > 0$, confirming its mechanical stability.

VALLEY POLARIZATION WITH IN-PLANE MAGNETIZATION

Janus engineering cannot destroy altermagnetism of Cr_2O_2 and $\text{V}_2\text{Se}_2\text{O}$ [28, 30]. Monolayer Fe_2MoS_4 and Fe_2MoSe_4 possess altermagnetism[41], and Janus $\text{Fe}_2\text{MoS}_2\text{Se}_2$ should also have altermagnetism. However, the Janus structure can induce an inherent electric field with the magnitude of about $0.84 \text{ V}/\text{\AA}$ for $\text{Fe}_2\text{MoS}_2\text{Se}_2$, which can be estimated by planar average of the electrostatic potential energy along out-of-plane direction (see Figure 2 (c)). The built-in electric field has important effects on the electronic structures, as we shall see in a while. This Mo atom leads to that two Fe atoms have the same surrounding atomic arrangement of Mo as a segment with different orientations, which plays a crucial role in generating the altermagnetism. If the Mo atom is removed, this altermagnetism will disappear. In other words, the two Fe-atom sublattices are related by M_{xy} mirror or C_{4z} rotational symmetry instead of any translation operation, giving rise to altermagnetism.

Without SOC, the energy band structures of $\text{Fe}_2\text{MoS}_2\text{Se}_2$ is plotted in Figure 2 (d), which shows two valleys at X and Y high-symmetry points for both con-

duction and valence bands. Due to $[C_2||C_{4z}]$ (The C_2 is the two-fold rotation perpendicular to the spin axis.), no valley and spin polarizations can be observed. States around X and Y points are dominated by two different Fe atoms with opposite spin, producing altermagnetism and spin-valley locking. Moreover, these bands along the Γ - X and Γ - Y show opposite spin character, implying d -wave altermagnetism[27, 28, 41]. The magnetic moments of two Fe atoms are strictly equal in size and opposite in direction, and they are $2.94 \mu_B$ and $-2.94 \mu_B$, respectively. The total magnetic moment of $\text{Fe}_2\text{MoS}_2\text{Se}_2$ is strictly $0.00 \mu_B$. These are confirmed by M_{xy} mirror or C_{4z} rotational symmetry.

Here, we also consider the electronic correlation effects on physical properties of $\text{Fe}_2\text{MoS}_2\text{Se}_2$ by changing U value. It is found that the lattice constants a increases with increasing U (0-4 eV), and the magnitude of the change is about 0.12 \AA from 0 eV to 4 eV. According to Figure 3 (a), when $U < 3.7$ eV, $\text{Fe}_2\text{MoS}_2\text{Se}_2$ always possesses AFM1 ground state. The AFM2 ordering becomes ground state with U being larger than 3.7 eV, and the $\text{Fe}_2\text{MoS}_2\text{Se}_2$ will lose altermagnetism. According to Figure 3 (b), the easy-axis of $\text{Fe}_2\text{MoS}_2\text{Se}_2$ is always out-of-plane within considered U range. The evolutions of energy band structures and energy bandgap as a function of U are plotted in Figure 4 and FIG.S5 of ESI, respectively. With increasing U , the main characteristics of energy band structures remain unchanged, and only the band gap increases. Compared with spin-

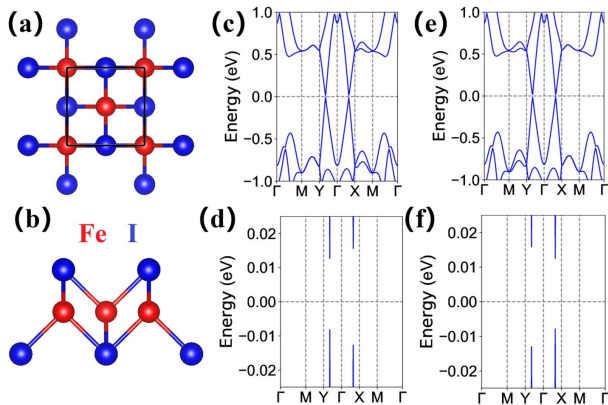


FIG. 6. (Color online) For Fe_2I_2 , (a) and (b): top and side views of the crystal structures; the energy band structures with SOC for magnetization direction along the positive x (c,d) and positive y (e,f) directions, respectively. The (d) and (f) show the enlarged portion of energy bands near the Fermi energy level for (c) and (e).

gapless Fe_2MoS_4 and Fe_2MoSe_4 (Weyl semimetal) with $U=0$ eV[41], $\text{Fe}_2\text{MoS}_2\text{Se}_2$ is a direct band gap semiconductor with gap value of 34 meV, which may be due to inherent electric field, not the effects of lattice constants (The a of $\text{Fe}_2\text{MoS}_2\text{Se}_2$ is between a of Fe_2MoS_4 and Fe_2MoSe_4).

With SOC, the energy band structures and topological properties of 2D systems depend on the magnetization direction, which can affect the symmetry of a system. For 2D hexagonal magnetic lattice, only out-of-plane magnetization allows valley polarization between -K and K valleys[20]. For Fe_2I_2 monolayer, quantum anomalous Hall effect can only be manifested in a magnetization direction that is perpendicular to the plane[42]. Strictly speaking, the projection of the magnetization direction possesses an out-of-plane component that facilitates the valley polarization and quantum anomalous Hall effect previously discussed. The energy band structures of $\text{Fe}_2\text{MoS}_2\text{Se}_2$ are plotted in Figure 5 without SOC and with SOC for magnetization direction along the positive z , positive x , and positive y directions. For out-of-plane case, the Y and X valleys have the same energy, giving rise to no valley polarization due to $C_{4z}T$ symmetry. For in-plane x direction, the valley polarization can be observed due to broken $C_{4z}T$ symmetry, and the spin polarization can also occur due to spin-valley locking. The valley splitting between Y and X valleys in the conduction bands is about 1.6 meV. When the magnetization direction changes from x to y , the valley polarization will be reversed. The energy band structures with in-plane xy direction is also calculated, which shows no valley polarization (see FIG.S6), being consistent with previous discussion.

The Y and X valleys of $\text{Fe}_2\text{MoS}_2\text{Se}_2$ are mainly from Fe character, which is a $3d$ element with a weak SOC.

To enhance valley splitting, the mass of this magnetic atom should be increased to strengthen the SOC, for example by using $4d$ or $5d$ elements. Similar strategy can also be found in hexagonal valley materials. From FeBr_2 to RuBr_2 , the valley splitting between -K and K valleys can be significantly enhanced[43, 44]. Here, an unrealistic material $\text{Ru}_2\text{MoS}_2\text{Se}_2$ is used to confirm our proposal (When U is less than 3.5 eV, this spin polarization calculation converges to a non-magnetic solution. Here, we use $U=4$ eV to obtain magnetic solution, and then calculate the related energy band structures). The energy band structures of $\text{Ru}_2\text{MoS}_2\text{Se}_2$ are shown in Figure 5 without SOC and with SOC for magnetization direction along the positive z , positive x , and positive y directions. It is clearly seen that $\text{Ru}_2\text{MoS}_2\text{Se}_2$ possesses an obvious valley splitting of 90 meV between Y_1 and X_1 valleys in the conduction bands for in-plane x magnetization. With the magnetization direction changing from x to y , the reversed valley polarization can be observed. Thus, the mass of the magnetic atoms determines the size of the valley splitting.

DISCUSSION AND CONCLUSION

In fact, our proposed method, analysis and results can be readily extended to 2D tetragonal FM materials, which can possess valley polarization with in-plane x or y magnetization. The Fe_2I_2 monolayer has been predicted to be a stable quantum anomalous Hall insulator with out-of-plane FM ordering[42], and it crystallizes in the $P4/nmm$ space group (No.129), which can be used to confirm our proposed way of realizing valley polarization. The crystal structures of Fe_2I_2 are shown in Figure 6 (a) and (b), which shows C_{4z} symmetry. The optimized equilibrium lattice constants are $a=b=3.863$ Å with $U=2.5$ eV. The energy band structures of Fe_2I_2 are plotted in Figure 6 (c,d,e,f) with SOC for magnetization direction along the positive x and positive y directions. A valley splitting can be observed for in-plane x or y direction, which can be reversed by switching the direction of magnetization between x and y . Therefore, our proposal can be extended to tetragonal magnetic systems.

In summary, a way of realizing valley polarization in 2D materials with in-plane magnetization is proposed in tetragonal lattice. By rotating in-plane magnetization, the valley polarization can be reversed. For 2D hexagonal magnetic lattice (both FM and AFM system) with valley physics at -K/K point, the SOC plus out-of-plane magnetization is required to produce valley polarization. For our proposed 2D tetragonal magnetic lattice, the combination of SOC and in-plane magnetization is essential for generating valley polarization. The valley splitting of tetragonal system with $3d$ magnetic atom is weak, and $4d$ or $5d$ tetragonal system should be further searched to achieve large valley polarization. These explored phe-

nomena not only enrich the valley physics but also expand valleytronic materials.

This work is supported by Natural Science Basis Research Plan in Shaanxi Province of China (2021JM-456). We are grateful to Shanxi Supercomputing Center of China, and the calculations were performed on TianHe-2.

* sandongyuwang@163.com

- [1] J. R. Schaibley, H. Yu, G. Clark, P. Rivera, J. S. Ross, K. L. Seyler, W. Yao and X. Xu, Valleytronics in 2D materials, *Nat. Rev. Mater.* **1**, 16055 (2016).
- [2] G. Pacchioni, Valleytronics with a twist, *Nat. Rev. Mater.* **5**, 480 (2020).
- [3] S. A. Vitale, D. Nezhich, J. O. Varghese, P. Kim, N. Gedik, P. Jarillo-Herrero, D. Xiao and M. Rothschild, Valleytronics: opportunities, challenges, and paths forward, *Small* **14**, 1801483 (2018).
- [4] D. Xiao, M. C. Chang and Q. Niu, Berry phase effects on electronic properties, *Rev. Mod. Phys.* **82**, 1959 (2010).
- [5] X. X. Zhang, Y. Lai, E. Dohner, S. Moon, T. Taniguchi, K. Watanabe, D. Smirnov and T. F. Heinz, Zeeman-Induced Valley-Sensitive Photocurrent in Monolayer MoS₂, *Phys. Rev. Lett.* **122**, 127401 (2019).
- [6] L. Xu, M. Yang, L. Shen, J. Zhou, T. Zhu and Y. P. Feng, Large valley splitting in monolayer WS₂ by proximity coupling to an insulating antiferromagnetic substrate, *Phys. Rev. B* **97**, 041405 (2018).
- [7] W. Zhou, Z. Yang, A. Li, M. Long and F. Ouyang, Spin and valley splittings in Janus monolayer WSSe on a MnO (111) surface: Large effective Zeeman field and opening of a helical gap, *Phys. Rev. B* **101**, 045113 (2020).
- [8] T. Cao, G. Wang, W. Han, H. Ye, C. Zhu, J. Shi, Q. Niu, P. Tan, E. Wang, B. Liu and J. Feng, Valley-selective circular dichroism of monolayer molybdenum disulphide, *Nat. Commun.* **3**, 887 (2012).
- [9] L. Xie and X. Cui, Manipulating spin-polarized photocurrents in 2D transition metal dichalcogenides, *Proc. Natl. Acad. Sci. USA* **113**, 3746 (2016).
- [10] W. Y. Tong, S. J. Gong, X. Wan and C. G. Duan, Concepts of ferrovalley material and anomalous valley Hall effect, *Nat. Commun.* **7**, 13612 (2016).
- [11] Y. B. Liu, T. Zhang, K. Y. Dou, W. H. Du, R. Peng, Y. Dai, B. B. Huang, and Y. D. Ma, Valley-Contrasting Physics in Single-Layer CrSi₂N₄ and CrSi₂P₄, *J. Phys. Chem. Lett.* **12**, 8341 (2021).
- [12] Z. Song, X. Sun, J. Zheng, F. Pan, Y. Hou, M.-H. Yung, J. Yang, and J. Lu, Spontaneous valley splitting and valley pseudospin field effect transistors of monolayer VAgP₂Se₆, *Nanoscale* **10**, 13986 (2018).
- [13] J. Zhou, Y. P. Feng, and L. Shen, Atomic-orbital-free intrinsic ferromagnetism in electrenes, *Phys. Rev. B* **102**, 180407(R) (2020).
- [14] P. Zhao, Y. Ma, C. Lei, H. Wang, B. Huang, and Y. Dai, Single-layer LaBr₂: Two-dimensional valleytronic semiconductor with spontaneous spin and valley polarizations, *Appl. Phys. Lett.* **115**, 261605 (2019).
- [15] X. Y. Feng, X. L. Xu, Z. L. He, R. Peng, Y. Dai, B. B. Huang and Y. D. Ma, Valley-related multiple Hall effect in monolayer VSi₂P₄, *Phys. Rev. B* **104**, 075421 (2021).
- [16] S. D. Guo, J. X. Zhu, W. Q. Mu and B. G. Liu, Possible way to achieve anomalous valley Hall effect by piezoelectric effect in a GdCl₂ monolayer, *Phys. Rev. B* **104**, 224428 (2021).
- [17] Y. Zang, Y. Ma, R. Peng, H. Wang, B. Huang, and Y. Dai, Large valley-polarized state in single-layer NbX₂ (X = S, Se): Theoretical prediction, *Nano Res.* **14**, 834 (2021).
- [18] R. Peng, Y. Ma, X. Xu, Z. He, B. Huang and Y. Dai, Intrinsic anomalous valley Hall effect in single-layer Nb₃I₈, *Phys. Rev. B* **102**, 035412 (2020).
- [19] W. Du, Y. Ma, R. Peng, H. Wang, B. Huang, and Y. Dai, Prediction of single-layer TiVI₆ as a promising two-dimensional valleytronic semiconductor with spontaneous valley polarization, *J. Mater. Chem. C* **8**, 13220 (2020).
- [20] R. Li, J. W. Jiang, W. B. Mi and H. L. Bai, Room temperature spontaneous valley polarization in two-dimensional FeClBr monolayer, *Nanoscale* **13**, 14807 (2021).
- [21] X. Hu, Half-metallic antiferromagnet as a prospective material for spintronics, *Adv. Mater.* **24**, 294 (2012).
- [22] T. Jungwirth, J. Sinova, A. Manchon, X. Marti, J. Wunderlich and C. Felser, The multiple directions of antiferromagnetic spintronics, *Nat. Phys.* **14**, 200 (2018).
- [23] S. D. Guo, Y. L. Tao, Z. Y. Zhuo, G. Zhu and Y. S. Ang, Electric-field-tuned anomalous valley Hall effect in A-type hexagonal antiferromagnetic monolayers, *Phys. Rev. B* **109**, 134402 (2024).
- [24] S. D. Guo, L. Zhang, Y. Zhang, P. Li and G. Wang, Large spontaneous valley polarization and anomalous valley Hall effect in antiferromagnetic monolayer Fe₂CF₂, *Phys. Rev. B* **110**, 024416 (2024).
- [25] L. Šmejkal, J. Sinova and T. Jungwirth, Beyond conventional ferromagnetism and antiferromagnetism: A phase with nonrelativistic spin and crystal rotation symmetry, *Phys. Rev. X* **12**, 031042 (2022).
- [26] I. Mazin, Altermagnetism: a new punch line of fundamental magnetism, *Phys. Rev. X* **12**, 040002 (2022).
- [27] H.-Y. Ma, M. L. Hu, N. N. Li, J. P. Liu, W. Yao, J. F. Jia and J. W. Liu, Multifunctional antiferromagnetic materials with giant piezomagnetism and noncollinear spin current, *Nat. Commun.* **12**, 2846 (2021).
- [28] S.-D. Guo, X.-S. Guo, K. Cheng, K. Wang, and Y. S. Ang, Piezoelectric altermagnetism and spin-valley polarization in Janus monolayer Cr₂SO, *Appl. Phys. Lett.* **123**, 082401 (2023).
- [29] X. Chen, D. Wang, L. Y. Li and B. Sanyal, Giant spin-splitting and tunable spin-momentum locked transport in room temperature collinear antiferromagnetic semimetallic CrO monolayer, *Appl. Phys. Lett.* **123**, 022402 (2023).
- [30] Y. Zhu, T. Chen, Y. Li, L. Qiao, X. Ma, C. Liu, T. Hu, H. Gao and W. Ren, Multipiezo Effect in Altermagnetic V₂SeTeO Monolayer, *Nano Lett.* **24**, 472 (2024).
- [31] Y. Wu, L. Deng, X. Yin, J. Tong, F. Tian and X. Zhang, Valley-Related Multipiezo Effect and Noncollinear Spin Current in an Altermagnet Fe₂Se₂O Monolayer, *Nano Lett.* **24**, 10534 (2024).
- [32] Y. Liu, J. Yu and C. C. Liu, Twisted Magnetic Van der Waals Bilayers: An Ideal Platform for Altermagnetism, *arXiv:2404.17146* (2024).
- [33] S. D. Guo, Y. Liu, J. Yu and C. C. Liu, Valley polarization in twisted altermagnetism, *arXiv:2406.13950* (2024).
- [34] R. W. Zhang, C. X. Cui, R. Z. Li, J. Y. Duan, L. Li, Z.

- M. Yu and Y. G. Yao, Predictable gate-field control of spin in altermagnets with spin-layer coupling, *Phys. Rev. Lett.* **133**, 056401 (2024).
- [35] P. Hohenberg and W. Kohn, Inhomogeneous Electron Gas, *Phys. Rev.* **136**, B864 (1964); W. Kohn and L. J. Sham, Self-Consistent Equations Including Exchange and Correlation Effects, *Phys. Rev.* **140**, A1133 (1965).
- [36] G. Kresse, Ab initio molecular dynamics for liquid metals, *J. Non-Cryst. Solids* **193**, 222 (1995).
- [37] G. Kresse and J. Furthmüller, Efficiency of ab-initio total energy calculations for metals and semiconductors using a plane-wave basis set, *Comput. Mater. Sci.* **6**, **15** (1996).
- [38] G. Kresse and D. Joubert, From ultrasoft pseudopotentials to the projector augmented-wave method, *Phys. Rev. B* **59**, 1758 (1999).
- [39] J. P. Perdew, K. Burke and M. Ernzerhof, Generalized gradient approximation made simple, *Phys. Rev. Lett.* **77**, 3865 (1996).
- [40] A. Togo, F. Oba and I. Tanaka, First-principles calculations of the ferroelastic transition between rutile-type and CaCl_2 -type SiO_2 at high pressures, *Phys. Rev. B* **78**, 134106 (2008).
- [41] C. Y. Tan, Z. F. Gao, H. C. Yang, K. Liu, P. J. Guo and Z. Y. Lu, Bipolarized Weyl semimetals and quantum crystal valley Hall effect in two-dimensional altermagnetic materials, arXiv:2406.16603 (2024).
- [42] Q. L. Sun, Y. D. Ma and N. Kioussis, Two-dimensional Dirac spin-gapless semiconductors with tunable perpendicular magnetic anisotropy and a robust quantum anomalous Hall effect, *Mater. Horiz.* **7**, 2071 (2020).
- [43] W. Pan, Tuning the magnetic anisotropy and topological phase with electronic correlation in single-layer $H\text{-FeBr}_2$, *Phys. Rev. B* **106**, 125122 (2022).
- [44] H. Huan, Y. Xue, B. Zhao, G. Y. Gao, H. R. Bao and Z. Q. Yang, Strain-induced half-valley metals and topological phase transitions in MBr_2 monolayers (M=Ru, OS), *Phys. Rev. B* **104**, 165427 (2021).